

Structure of polydisperse inverse ferrofluids: Theory and computer simulation

Y. C. Jian, Y. Gao and J. P. Huang*

*Surface Physics Laboratory and Department of Physics,
Fudan University, Shanghai 200433, China*

R. Tao

Department of Physics, Temple University, Philadelphia, Pennsylvania 19122

(Dated: August 30, 2018)

Abstract

By using theoretical analysis and molecular dynamics simulations, we investigate the structure of colloidal crystals formed by nonmagnetic microparticles (or *magnetic holes*) suspended in ferrofluids (called *inverse ferrofluids*), by taking into account the effect of polydispersity in size of the nonmagnetic microparticles. Such polydispersity often exists in real situations. We obtain an analytical expression for the interaction energy of monodisperse, bidisperse, and polydisperse inverse ferrofluids. Body-centered tetragonal (*bct*) lattices are shown to possess the lowest energy when compared with other sorts of lattices, and thus serve as the ground state of the systems. Also, the effect of microparticle size distributions (namely, polydispersity in size) plays an important role in the formation of various kinds of structural configurations. Thus, it seems possible to fabricate colloidal crystals by choosing appropriate polydispersity in size.

* Corresponding author. Electronic address: jphuang@fudan.edu.cn

I. INTRODUCTION

In recent years, inverse ferrofluids with nonmagnetic colloidal microparticles suspended in a host ferrofluid (also called magnetic fluid)¹⁻³ have drawn considerable attention for its potential application in its industrial applications and potential use in biomedicine.⁴⁻¹¹ The size of the non-magnetic microparticles are about $1 \sim 100 \mu\text{m}$, which can be easily made in experiments, such as polystyrene microparticles. The inverse ferrofluid system can be modelled in a dipolar interaction approximation. Here, the dipolar interaction approximation is actually the first-order approximation of multipolar interaction. Because the nonmagnetic microparticles are much larger than the ferromagnetic nanoparticles in a host ferrofluid, the host can theoretically be treated as a uniform continuum background in which the much larger nonmagnetic microparticles are embedded. If an external magnetic field is applied to the inverse ferrofluid, the nonmagnetic microparticles suspended in the host ferrofluid can be seen to possess an effective magnetic moment but opposite in direction to the magnetization of the host ferrofluid. As the external magnetic field increases, the nonmagnetic microparticles aggregate and form chains parallel with the applied magnetic field. These chains finally aggregate to a column-like structure, completing a phase transition process, which is similar to the cases of electrorheological fluids and magnetorheological fluids under external electric or magnetic fields. The columns can behave as different structures like body-centered tetragonal (*bct*) lattices, face centered cubic (*fcc*) lattices, hexagonal close packed (*hcp*) lattices, and so on. In this work, we assume that the external magnetic field is large enough to form different lattice structures. The actual value of the external magnetic field needed to form such structures is related to the volume fraction of the nonmagnetic microparticles and the magnetic properties of the host ferrofluid.

In this work, we shall use the dipole-multipole interaction model¹² to investigate the structure of inverse ferrofluids. In ref 12, Zhang and Widom discussed how the geometry of elongated microparticles will affect the interaction between two droplets, and introduced higher multipole moments' contribution by using a dipole and multipole (dipole-multipole) interaction model to give a more exact expression of interaction energy than using the dipole and dipole (dipole-dipole) interaction model. The leading dipole-dipole force does not reflect the geometry relation between the microparticles nearby, while the dipole-multipole model includes the contributions from the size mismatch and is simpler and practical than the multipolar expansion theory^{13,14} in dealing with the complex interaction between microparticles for its accuracy. Size distributions can be regarded

as a crucial factor which causes depletion forces in colloidal droplets.¹⁵ Even though researchers have tried their efforts to fabricate monodisperse systems for obtaining optimal physical or chemical properties,^{16,17} polydispersity in size of microparticles often exists in real situations,^{18–22} since the microparticles always possess a Gaussian or log-normal distribution. Here we consider size distributions as an extra factor affecting the interaction energy. Polydisperse ferrofluid models are usually treated in a global perspective using chemical potential or free energy methods,^{6,23,24} while the current model concerns the local nature in the crystal background. A brief modelling is carried out for the size distribution picture in the formation of crystal lattices. The purpose of this paper is to use this model to treat the structure formation in monodisperse, bidisperse, and polydisperse inverse ferrofluids, thus yielding theoretical predictions for the ground state for the systems with or without microparticle size distributions (or polydispersity in size). It is found that when the size mismatch is considered between the microparticles, the interaction between them becomes complex and sensitive to the different configurations. This method can also be extended to other ordered configurations in polydisperse crystal systems.

This paper is organized as follows. In Section II, based on the dipole-multipole interaction model, we present the basic two-microparticle interaction model to derive interaction potentials. In Sections III and IV, we apply the model to three typical structures of colloid crystals formed in inverse ferrofluids, and then investigate the ground state in two different configurations by taking into account the effect of size distributions. As an illustration, in Section V we perform molecular dynamics simulations to give a picture of the microparticle size distribution in the formation of a *bct* lattice in bidisperse inverse ferrofluids. The paper ends with a discussion and conclusion in Section VI.

II. INTERACTION MODEL FOR TWO NONMAGNETIC MICROPARTICLES

We start by considering a simple situation in which two nonmagnetic spherical microparticles (or called *magnetic holes*) are put nearby inside a ferrofluid which is homogeneous at the scale of a sphere in an applied uniform magnetic field H , see Figure 1. The nonmagnetic microparticles create holes in the ferrofluid, and corresponding to the amount and susceptibility of the ferrofluid, they possess the effective magnetic moment, which can be described by²⁵ $\mathbf{m} = -\frac{\chi_f}{1+\frac{2}{3}\chi_f}V\mathbf{H} = -\chi V\mathbf{H}$, where χ_f (or χ) means the magnetic susceptibility of the host (or inverse) ferrofluid. When the two nonmagnetic microparticles placed together with distance r_{ij} away, we can view

the magnetization in one sphere (labelled as A) is induced by the second (B). The central point of dipole-multipole technique is to treat B as the dipole moment m at the first place, and then examine the surface charge density Σ induced on the sphere A. From Σ we can use the multipole expansion (detailed discussion can be found in ref 26) to obtain the multipole moment. When exchanging the status of A and B, treating A as the dipole moment, the averaged force between the two microparticles is thus obtained. For the perturbation of the magnetic field due to the two microparticles, magnetization M in the microparticles become nonuniform, and they will obtain multipole moments from mutual induction. However, the bulk magnetic charge density still satisfies $\rho = \nabla \cdot \mathbf{M} = 0$. So we need only study the surface charge Σ_n ,

$$\Sigma_n = \hat{\mathbf{n}} \cdot \mathbf{M}, \quad (1)$$

where $\hat{\mathbf{n}}$ is the unit normal vector pointing outwards. The magnetic multipole moments by surface charge density in spherical coordinates can be written as,

$$q_{ln} = \int Y_{ln}^*(\phi, \varphi) r_1^l \Sigma_n dS, \quad (2)$$

where r_1 denotes the radius of the microparticle. All $n \neq 0$ moments vanish due to rotational symmetry about the direction of magnetization, so eq 2 can be rewritten as

$$A_l \equiv q_{l0} = \sqrt{(2l+1)\pi} \int_{-1}^1 P_l(\cos \phi) r_1^{l+2} \Sigma_n(\cos \phi) d \cos \phi. \quad (3)$$

We can expand the surface charge density in Legendre polynomials in the spherical coordinates (r, ϕ, φ) ,¹²

$$\Sigma_n(\cos \phi) = \frac{\chi}{r_{ij}^3} \sum_{l=1}^{\infty} (-1)^{l+1} l(l+1) \left(\frac{r_1}{r_{ij}} \right)^{l-1} P_l(\cos \phi). \quad (4)$$

The $l \geq 2$ parts in eq 4 correspond to the effects of multipole (that are beyond the dipole). Here we set spherical harmonics $\int_0^{2\pi} d\varphi \int_0^\pi \sin \phi Y_{l',n'}^*(\phi, \varphi) Y_l(\phi, \varphi) d\phi = \delta_{l',l} \delta_{n',n}$. The force between the dipole moment m and induced multipole moment A_l can be derived as

$$F_{D-M} = (-1)^l (l+1)(l+2) \left(\frac{4\pi}{2l+1} \right)^{\frac{1}{2}} \frac{mA_l}{r_{ij}^{l+3}} \cos \phi. \quad (5)$$

In view of the orthogonal relation $\int_{-1}^1 P_l^n P_{l'}^n dx = \frac{2}{2l+1} \frac{(l+n)!}{(l-n)!} \delta_{ll'}$, we obtain the interaction energy for the dipole-multipole moment

$$U_{D-M} = \frac{\pi}{4} \mu_f m_1 m_2 \sum_l \frac{\pi}{2} \chi \frac{l(l+1)^2}{2l+1} (r_1^{2l+1} + r_2^{2l+1}) \frac{1-3\cos^2 \theta}{r_{ij}^{2l+4}} = \mu \sum_l f(l) \frac{1-3\cos^2 \theta}{r_{ij}^{2l+4}}, \quad (6)$$

where $\mu = \frac{\pi}{4}\mu_f m_1 m_2$, $f(l) = \frac{\pi}{2}\chi \frac{l(l+1)^2}{2l+1}(r_1^{2l+1} + r_2^{2l+1})$, the suffix $D(M)$ of force F or energy U stands for the dipole moment (multipole moment), and magnetic permeability $\mu_f = \mu_0(1 + \chi_f)$ with $\mu_0 = 4\pi \times 10^{-7} \text{ H}\cdot\text{m}^{-1}$. Here m_1 and m_2 denote the effective magnetic moments of the two nonmagnetic microparticles, which is induced by external field as dipolar perturbation. $0 \leq \theta \leq \frac{\pi}{2}$ is the angle between the their joint line with the direction of external field, and ϕ and φ are both the spherical coordinates (r, ϕ, φ) for one single nonmagnetic microparticle. For typical ferrofluids, there are magnetic susceptibilities, $\chi_f = 1.9$ and $\chi = 0.836$.²³ Because we consider the *bct*, *fcc* and *hcp* lattices, the crystal rotational symmetry in the *xy* plane is fourfold, and the value of n can only be $0, \pm 4, \dots$. In the general case, when the polarizabilities between the microparticles and ambient fluid is low, the higher magnetic moments can be neglected since they contribute less than 5 percent of the total energy.¹² In this picture, the nonmagnetic microparticle pair reflects the dipole-dipole and dipole-multipole nature of the interaction, and can be used to predict the behavior of microparticle chains in simple crystals.

III. POSSIBLE GROUND STATE FOR UNIFORM ORDERED CONFIGURATIONS

Let us first consider a bidisperse model which has been widely used in the study of magnetorheological fluids and ferrofluids. The model has large amount of spherical nonmagnetic microparticles with two different sizes suspended in a ferrofluid which is confined between two infinite parallel nonmagnetic plates with positions at $z = 0$ and $z = L$, respectively. When a magnetic field is applied, dipole and multipole moments will be induced to appear in the spheres. The inverse ferrofluid systems consist of spherical nonmagnetic microparticles in a carrier ferrofluid, and the viscosity of the whole inverse ferrofluid increases dramatically in the presence of an applied magnetic field. If the magnetic field exceeds a critical value, the system turns into a solid whose yield stress increases as the exerting field is further strengthened. The induced solid structure is supposed to be the configuration minimizing the interaction energy, and here we assume first that the microparticles with two different size have a fixed distribution as discussed below.

Using the cylindrical coordinates, the interaction energy between two microparticles labelled as i and j considering both the dipole-dipole and dipole-multipole effects can be written as

$$U_{ij}(\rho, z) = \mu \left(1 + \sum_l \frac{f(l)}{r_{ij}^{2l+1}} \right) \cdot \left(\frac{1 - 3 \cos^2 \theta}{r_{ij}^3} \right), \quad (7)$$

where the center-to-center separation $r_{ij} = |r_i - r_j| = [\rho^2 + (z_i - z_j)^2]^{\frac{1}{2}}$, and θ is the angle between

the field and separation vector r_{ij} (see Figure 1). Here $\rho = [(x_i - x_j)^2 + (y_i - y_j)^2]^{\frac{1}{2}}$ stands for the distance between chain A and chain B (Figure 2), and z_i denotes the vertical shift of the position of microparticles. Since the inverse ferrofluid is confined between two plates, the microparticle dipole at (x, y, z) and its images at $(x, y, 2Lj \pm z)$ for $j = \pm 1, \pm 2, \dots$ constitute an infinite chain. In this work, we would discuss the physical infinite chains. After applying a strong magnetic field, the mismatch between the spheres and the host ferrofluid, as well as the different sizes of the two sorts of spheres will make the spheres aggregate into lattices like a bct (body-centered tetragonal) lattice. In fact, the bct lattice can be regarded as a compound of chains of A and B, where chains B are obtained from chains A by shifting a distance r_1 (microparticle radius) in the field direction. Thus, we shall study the case in which the identical nonmagnetic microparticles gather together to form a uniform chain, when phase separation or transition happens. For long range interactions, the individual colloidal microparticles can be made nontouching when they are charged and stabilized by electric or magnetic static forces, with a low volume fraction of nonmagnetic microparticles. The interaction energy between the nonmagnetic microparticles can be divided into two parts: one is from the self energy of one chain (U_s), the other is from the interaction between different chains ($U_{ij}(\rho, z)$). Consider the nonmagnetic microparticles along one chain at $r_j = 2aj\hat{z}$ ($j = 0, \pm 1, \pm 2, \dots$) (namely, chain A), and the other chain at $r_j = (2j + 1)a\hat{z}$ (chain B), the average self energy per microparticle in an infinite chain is $U_s = -\mu \sum_{s=1}^{\infty} [\frac{1}{(2as)^3} + 2 \sum_l \frac{f(l)}{(2as)^{2l+4}}]$.

If we notice that for an infinite chain all even multipole contributions vanish due to spatial magnetic antisymmetry around the spheres, the sum starts at $l = 3$. Because the radius of the sphere is smaller than the lattice parameter a , for large multipole moment, $\frac{r_1^{2l+1} + r_2^{2l+1}}{(2a)^{2l}} \ll 1$, we need only consider the first two moment contributions for simplicity. Thus the average self energy U_s can be calculated as $U_s = -2\mu(\frac{\zeta(3)}{(2a)^3} + \frac{f(3)\zeta(6)}{(2a)^6} + \frac{f(5)\zeta(10)}{(2a)^{10}}) = -\mu(\frac{0.300514}{a^3} + \frac{0.0317920f(3)}{a^6} + \frac{0.00195507f(5)}{a^{10}})$, where $\zeta(n) = \sum_{s=1}^{\infty} \frac{1}{s^n}$ is the Riemann ζ function. The interaction energy between two parallel infinite chains can be given by $\frac{1}{2}U_{ij}(\rho, z)$, in which the microparticles along one chain locate at $r_j = 2aj\hat{z}$ ($j = 0, \pm 1, \pm 2, \dots$) and one microparticle locates at $r_j = \rho + z\hat{z}$,

$$\begin{aligned}
U_{ij}(\rho, z) &= -\mu[(2 + \rho \frac{\partial}{\partial \rho}) \sum_{j=-\infty}^{\infty} \frac{1}{[\rho^2 + (z - 2ja)^2]^{\frac{3}{2}}}] \\
&\quad - \mu[\sum_l f(l)(2 + \frac{3}{2l+2}\rho \frac{\partial}{\partial \rho}) \sum_{j=-\infty}^{\infty} \frac{1}{[\rho^2 + (z - 2ja)^2]^{l+2}}] \\
&= U_1 + U_2.
\end{aligned} \tag{8}$$

Following the Fourier expanding technique which is proposed by Tao *et al.*,²⁷ we derive U_2

which is the second part of $U_{ij}(\rho, z)$ as

$$U_2 = -\mu \sum_l \frac{f(l)}{4a\rho^{2l+3}} \left[-\frac{(2l+1)\sqrt{\pi}\Gamma(l+\frac{3}{2})}{\Gamma(l+3)} + 2^{\frac{1}{2}-l} \left(\frac{s\rho}{a}\right)^{l+\frac{3}{2}} \pi^{l+2} \cos\left(\frac{s\pi z}{a}\right) \cdot S \right] \quad (9)$$

with

$$S = \sum_{s=1}^{\infty} \left(\frac{K_{\frac{5}{2}}\left(\frac{s\pi}{\rho}\right)}{\Gamma(l+3)} + \frac{4K_{\frac{3}{2}}\left(\frac{s\pi}{\rho}\right)}{\Gamma(l+2)} \right). \quad (10)$$

Here $K_i(x)$ represents the i th order modified Bessel function, $\Gamma(x)$ the Γ function, and s denotes the index in Fourier transformation.²⁶ And the dipole-dipole energy U_1 is written as

$$U_1 = -\frac{\mu}{a^3} \sum_{s=1}^{\infty} 2\pi^2 s^2 K_0\left(\frac{s\pi\rho}{a}\right) \cos\left(\frac{s\pi z}{a}\right). \quad (11)$$

We obtain the expression for $U_{ij}(\rho, z)$, and the interaction energy per nonmagnetic microparticle $U(\rho, z)$ is $U_s + \frac{1}{2} \sum_k U_{ij}(\rho, z)$, where \sum_k denotes the summation over all chains except the considered microparticle. For the same reason of approximation discussed above, we need only choose the first two terms ($l = 3$ and $l = 5$) in the calculation.

The interaction between chain A and chain B depends on the shift z , the lattice structure and the nonmagnetic microparticle size. An estimation of the interaction energy per nonmagnetic microparticle includes the nearest and next-nearest neighboring chains, here we could discuss three most common lattice structures: *bct*, *fcc*, and *hcp* lattices. For the above lattices, their corresponding energy of $U_{ij}(\rho, z)$ can be respectively approximated as $U_{ij,bct}(\rho, z) = 4U_{ij}(\sqrt{3}a, z=0) - 4U_{ij}(\sqrt{6}a, z=0)$, $U_{ij,fcc}(\rho, z) = 4U_{ij}(\sqrt{3}a, z=0) - 2U_{ij}(2a, z=0)$, and $U_{ij,hcp}(\rho, z) = 3U_{ij}(\sqrt{3}a, z=0) - 4U_{ij}(2a, z=0)$.

Figure 3 shows, for different lattices, the dependence of $U_{ij}(\rho, z)$ on the vertical position shift z , which determines whether the interaction is attractive or repulsive. $U_{ij}(\rho, z)$ reflects the energy difference between chain A and chain B for (a) *bct*, (b) *fcc*, and (c) *hcp* lattices. It is evident that, for the same lattice structure, $U_{ij}(\rho, z)$ is minimized when the size difference between chain A and chain B is the smallest. For the sake of comparison, we also plot the results obtained by considering the dipole-dipole interaction only. Comparing the different lattices, we find that the *bct* lattice possesses the smallest energy at the equilibrium point, thus being the most stable.

Figure 4 displays the interaction energy $U(\rho, z)$ as a function of the lattice constant a for the *bct* lattice. It is shown that as the lattice constant increases, the dipole-multipole effect becomes weaker and weaker, and eventually it reduces to the dipole-dipole effect. In other words, as the lattice constant is smaller, one should take into account the dipole-multipole effect. In this case, the effect of polydispersity in size can also play an important role.

Figure 5 displays the interaction energy per nonmagnetic microparticle $U(\rho, z)$ vs the lattice parameter a for different lattice structures. The *bct* structure also proves to be the most stable state while the *hcp* lattice has the highest energy. It also shows that the energy gap between *bct* lattice and *fcc* lattice exists but is small. Figure 6(a) shows that the energy gap $\Delta U = U_{bct} - U_{fcc}$ is about 0.5 percent of the interaction energy value. In this aspect, the *bct* lattice proves always to be a more stable structure comparing with *fcc*. As the radius of microparticles increases, the energy gap between *bct* and *fcc* lattice enlarges accordingly. That is, the *bct* lattice becomes much more stable. Figure 6(b) shows the *bct* lattice energy $U(\rho, z)$ in respect of different sizes of microparticles for chain A and chain B. It can be seen that the close touching packing ($r_1 = r_2 = a$) has the lowest energy state. However, also from the graph, the crystal with the same microparticle size (monodisperse system) may not be the lowest energy state, which gives a possible way of fabricating different crystals by tuning the distribution of microparticle size.

IV. POLYDISPERSE SYSTEM WITH RANDOM DISTRIBUTIONS

In Section III, we have discussed the structure and interaction in a bidisperse inverse ferrofluid (namely, containing microparticles with two different sizes). But the interaction form in polydisperse crystal system is complex and sensitive to the microstructure in the process of crystal formation. Now we investigate the structure of polydisperse inverse ferrofluids with microparticles of different sizes in a random configuration. To proceed, we assume that the average radius r satisfies the Gaussian distribution

$$P(r) = \frac{1}{\sqrt{2\pi}\sigma} \exp\left(-\frac{(r - r_0)^2}{2\sigma^2}\right), \quad (12)$$

where σ denotes the standard deviation of the distribution of microparticle radius, which describes the degree of polydispersity. Integrating eq 9 by r_1 and r_2 , we could get the average dipole-multipole energy \bar{U}_2 . Doing the same calculation to self energy U_s , we can get the average interaction energy $\bar{U}(\rho, z) = \bar{U}_s + U_1 + \bar{U}_2$, where the microparticle size r_1 and r_2 are replaced by the mean radius r_0 . The microparticle sizes will be distributed in a wider range as long as a larger σ is chosen.

Figure 7(a) shows the ground state interaction energy of *bct* lattice for different polydisperse distributions. As the degree of polydispersity σ increases, the energy $U(\rho, z)$ drops fast, especially when the distribution of microparticle size gathers around $r = a$. It shows that the inverse fer-

rofluid crystal in the formation of ground state tends to include microparticles possessing more different sizes. The crystal configuration energy of two uniform chains with identical microparticle aggregation is also plotted in the graph. Here we consider two cases. First, we assume the microparticles in chain A and chain B are identical, $r_1 = r_2 = r_0$. As r_0 increases, the behavior of energy decreasing is discovered to be similar with the random configuration with $\sigma = 0.2r_0$. Second, we set for one chain, such as chain B, the microparticle size $r_2 = a$ to be unchanged, while the microparticle size r_1 of chain A increases. It shows that the *bct* lattice energy for the second case is lower than the first case and two other random configurations. And it also shows that the random configuration is not always the state with the lowest energy. It proves that polydisperse systems are sensitive to many factors which can determine the microstructure. Figure 7(b) shows the energy gap between *bct* and *fcc* lattices for different distribution deviation σ . It is evident that higher σ leads to larger energy difference between *bct* and *fcc*, especially at larger r_0 . In other words, at larger r_0 and/or σ , *bct* lattices are much more stable than *fcc*.

V. MOLECULAR-DYNAMIC SIMULATIONS

Here we use a molecular-dynamic simulation, which was proposed by Tao *et al.*,²⁸ in order to briefly discuss the structure formation of bidisperse inverse ferrofluids. The simulation herein involves dipolar forces, multipole forces, viscous drag forces and the Brownian force. The microparticles are confined in a cell between two parallel magnetic pole plates, and they are randomly distributed initially, as shown in Figure 8(a). The motion of a microparticle i is described by a Langevin equation,

$$m_a \frac{d^2 \vec{r}_i}{dt^2} = \vec{F}_i - 3\pi\sigma\eta \frac{d\vec{r}_i}{dt} + \vec{R}_i(t), \quad (13)$$

where the second term in the right-hand side is the Stokes's drag force, R_i is the Brownian force, and

$$F_i = \sum_{i \neq j} (f_{ij} + f_{ij}^{rep}) + f_i^{wall}. \quad (14)$$

Here $f_{ij} = -\nabla U(\rho, z)$, while f_{ij}^{rep} , f_i^{wall} and $R_i(t)$, have the similar expressions as those in ref 27 and the references therein. In eq 13, m_a and σ are respectively the average mass and diameter of microparticles. Figure 8 shows the inverse ferrofluid structure with the parameters, magnetic field $H = 14$ Oe, temperature $T = 300$ K, $A' \equiv \frac{\mu_f m_1 m_2}{3\pi^2 \sigma^6 \eta^2} m_a = 10^{-2}$, and $B' \equiv \frac{\sqrt{6\pi k_B T \sigma^9 \eta / \tau}}{3\mu_f m_1 m_2} = 10^{-4}$. Here A' denotes the ratio of a dipolar force to a viscous force, B' the ratio of Brownian force to a

dipolar force, k_B the Boltzmann constant, and τ the subinterval time step.

We take into account a bidisperses system that contains two kinds of microparticles with different sizes, as shown in Figure 8. In details, this figure displays the configuration of microparticle distribution in a bidisperse system at (a) the initial state, (b) the state after 15 000 time steps, and (c) the state after 80 000 time steps. The order of Figure 8(c) is better than Figure 8(b). Here we should remark that 80 000 steps give the sufficient long time steps to reach the equilibrium state for the case of our interest. The structure for the bi-disperse system in Figure 8(b) and (c) has the following features: (i) In the field direction, the large spheres form the main chains from one plate to the other, where the large spheres touch each other. (ii) The large spheres also form many small *bct* lattice grains. However, they do not form a large *bct* lattice. (iii) The small spheres fill the gaps between these *bct* lattice grains. From Figure 8, it is observed that, for the parameters currently used, the order of a bidisperse system (which is a *bct*-like structure) is not as good as that of monodisperse system (no configurations shown herein). We should remark that the long-range interaction can yield the above-mentioned *bct* lattice structure, but some perturbations caused by the Brownian movement existing in the system can change it to another lattice structure which has similar free energy. Therefore, for the bi-disperse system of our interest, the large spheres form the main chains from one plate to the other in the field direction, thus forming many small *bct*-like lattice structures. While small spheres fill the gaps between these *bct*-like lattices, they themselves do not form a *bct*-like lattice due to such perturbations. Here we should also mention that the degree of order of a specific system depends on the choice of various physical parameters, for example, the size of microparticles and so forth.

VI. SUMMARY

In summary, by using theoretical analysis and molecular dynamics simulations, we investigate the structure of colloidal crystals formed by nonmagnetic microparticles (or magnetic holes) suspended in a host ferrofluid, by taking into account the effect of polydispersity in size of the nonmagnetic microparticles. We obtain an analytical expression for the interaction energy of monodisperse, bidisperse, and polydisperse inverse ferrofluids. The *bct* lattices are shown to possess the lowest energy when compared with other sorts of lattices, and thus serve as the ground state of the systems. Also, the effect of microparticle size distributions (namely, polydispersity in size) plays an important role in the formation of various kinds of structural configurations. Thus, it seems

possible to fabricate colloidal crystals by choosing appropriate polydispersity in size. As a matter of fact, it is straightforward to extend the present model to more ordered periodic systems,²⁹ in which the commensurate spacings can be chosen as equal or different.

Acknowledgments

Two of us (Y.C.J. and J.P.H.) are grateful to Dr. Hua Sun for valuable discussion. This work was supported by the National Natural Science Foundation of China under Grant No. 10604014, by the Shanghai Education Committee and the Shanghai Education Development Foundation ("Shu Guang" project), by the Pujiang Talent Project (No. 06PJ14006) of the Shanghai Science and Technology Committee, and by Chinese National Key Basic Research Special Fund under Grant No. 2006CB921706. Y.C.J. acknowledges the financial support by Tang Research Funds of Fudan University, and by the "Chun Tsung" Scholar Program of Fudan University.

References and Notes

- (1) Odenbach S., *Magnetoviscous Effects in Ferrofluids* Springer, Berlin, 2002.
- (2) Meriguet G.; Cousin F.; Dubois E.; Boue F.; Cebers A.; Farago B.; and Perzynski W. *J. Phys. Chem. B* **2006**, 110, 4378.
- (3) Sahoo Y.; Goodarzi A.; Swihart M. T.; Ohulchanskyy T. Y.; Kaur N.; Furlani E. P.; and Prasad P. N. *J. Phys. Chem. B* **2005**, 109, 3879.
- (4) Toussaint R.; Akselvoll J.; Helgesen G.; Skjeltorp A. T.; and Flekkøy E. G. *Phys. Rev. E* **2004**, 69, 011407.
- (5) Skjeltorp A. T. *Phys. Rev. Lett.* **1983**, 51, 2306.
- (6) Zubarev A. Y. and Iskakova L. Y. *Physica A* **2003**, 335, 314.
- (7) Chantrell R. and Wohlfart E. *J. Magn. Magn. Mater.* **1983**, 40, 1.
- (8) Rosensweig R. E. *Annu. Rev. Fluid Mech.* **1987**, 19, 437.
- (9) Ugelstad J. et al, *Blood Purif.* **1993**, 11, 349.
- (10) Hayter J. B.; Pynn R.; Charles S.; Skjeltorp A. T.; Trehwella J.; Stubbs G.; and Timmins P. *Phys. Rev. Lett.* **1989**, 62, 1667.
- (11) Koenig A.; Hébraud P.; Gosse C.; Dreyfus R.; Baudry J.; Bertrand E.; and Bibette J. *Phys. Rev. Lett.* **2005**, 95, 128301.
- (12) Zhang H. and Widom M. *Phys. Rev. E* **1995**, 51, 2099.
- (13) Friedberg R. and Yu Y. K. *Phys. Rev. B* **1992**, 46, 6582.
- (14) Clercx H. J. H. and Bossis G. *Phys. Rev. B* **1993**, 48, 2721.
- (15) Mondain-Monval O.; Leal-Calderon F.; Philip J.; and Bibette J. *Phys. Rev. Lett.* **1995**, 75, 3364.
- (16) Sacanna S. and Philipse A. P. *Langmuir* **2006**, 22, 10209.
- (17) Claesson E. M. and Philipse A. P. *Langmuir* **2005**, 21, 9412.
- (18) Dai Q. Q.; Li D. M.; Chen H. Y.; Kan S. H.; Li H. D.; Gao S. Y.; Hou Y. Y.; Liu B. B. and Zou G. T. *J. Phys. Chem. B* **2006**, 110, 16508.
- (19) Ethayaraja M.; Dutta K.; and Bandyopadhyaya R. *J. Phys. Chem. B* **2006**, 110, 16471.
- (20) Jodin L.; Dupuis A. C.; Rouviere E.; and Reiss P. *J. Phys. Chem. B* **2006**, 110, 7328.
- (21) Gao L. and Li Z. Y. *J. Appl. Phys.* **2002**, 91, 2045.
- (22) Wei E. B.; Poon Y. M.; Shin F. G.; and Gu G. Q. *Phys. Rev. B* **2006**, 74, 014107.
- (23) Kristóf T. and Szalai I. *Phys. Rev. E* **2003**, 68, 041109.

- (24) Huang J. P. and Holm C. *Phys. Rev. E* **2004**, 70, 061404.
- (25) J. Černák, G. Helgesen, and A. T. Skjeltorp, *Phys. Rev. E* **2004**, 70, 031504.
- (26) Jackson J. D., *Classical Electrodynamics*, 3rd edition Wiley, New York, 1999, Chapter 4.
- (27) Tao R. and Sun J. M. *Phys. Rev. Lett.* **1991**, 67, 398.
- (28) Tao R. and Jiang Q. *Phys. Rev. Lett.* **1994**, 73, 205.
- (29) Gross M. and Wei C. *Phys. Rev. E* **2000**, 61, 2099.

Figure captions

Figure 1. Schematic graph showing two nonmagnetic microparticles (magnetic hole) of radius r_1 and r_2 , suspended in a ferrofluid under an applied magnetic field H .

Figure 2. Three different lattices, bct , fcc , and hcp , which are composed of non-touching microparticles with different size distribution.

Figure 3. The dependence of interaction energy $U_I(\rho, z)$ (in units of μ_0) versus vertical shift z for different lattices: (a) bct , (b) fcc , and (c) hcp . In the legend, "dipole-dipole" denotes the case that the dipole-dipole interaction is only considered for calculating the interaction energy.

Figure 4. The interaction energy $U(\rho, z)$ versus lattice constant a . The solid line stands for the case in which the dipole-dipole interaction is only considered.

Figure 5. The interaction energy per microparticle $U(\rho, z)$ versus lattice constant a for different lattices, bct , fcc , and hcp .

Figure 6. (a) The energy gap $\Delta U = U_{bct} - U_{fcc}$ (in units of μ_0) versus different size of nonmagnetic microparticles in chain A and chain B; (b) The bct lattice energy $U(\rho, z)$ (in units of μ_0) versus different sizes of nonmagnetic microparticles in chain A and chain B.

Figure 7. (a) The ground state interaction energy of a bct lattice versus microparticle size r_0 for random polydispersity configuration (solid, dashed, and dotted lines) and a configuration composed of two different uniform chains (dash-dotted and short-dash-dotted lines). (b) The energy gap ΔU between bct and fcc lattices for random polydispersity versus r_0 .

Figure 8. The configuration of nonmagnetic microparticle distribution at (a) the initial state, (b) the state after 15000 time steps, and (c) the state after 80000 time steps.

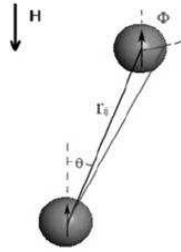


FIG. 1: Jian, Gao, Huang, and Tao

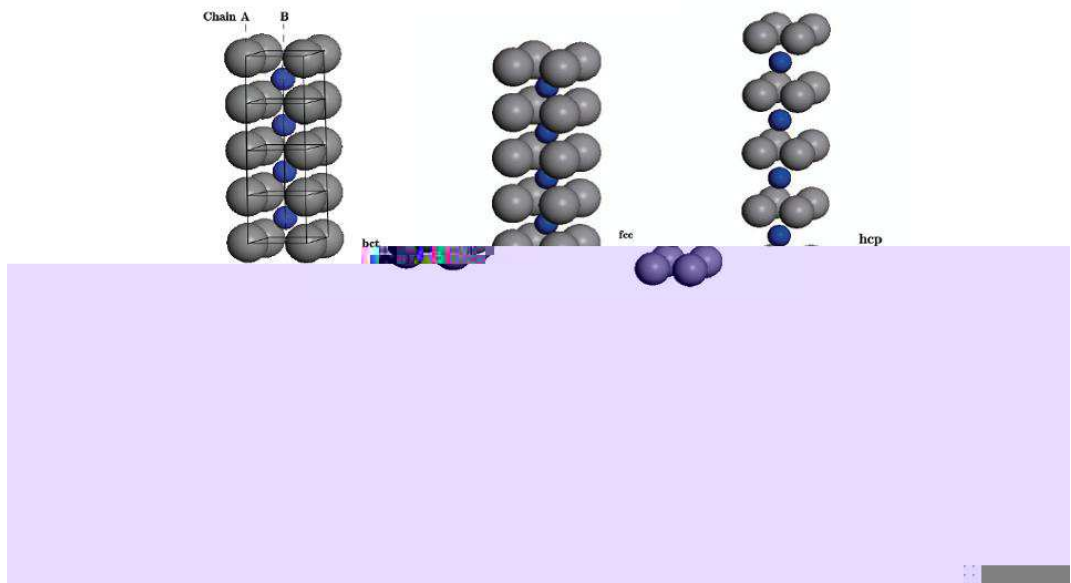


FIG. 2: Jian, Gao, Huang, and Tao

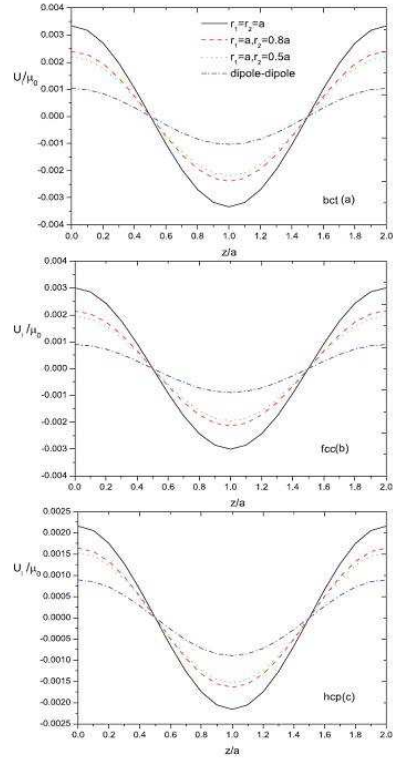


FIG. 3: Jian, Gao, Huang, and Tao

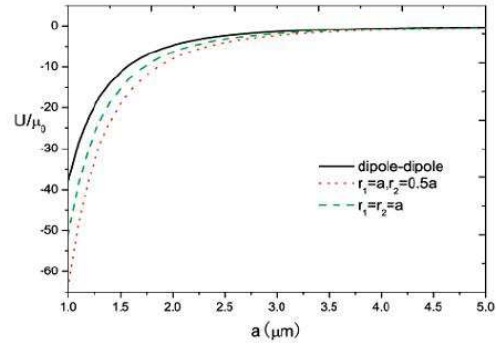


FIG. 4: Jian, Gao, Huang, and Tao

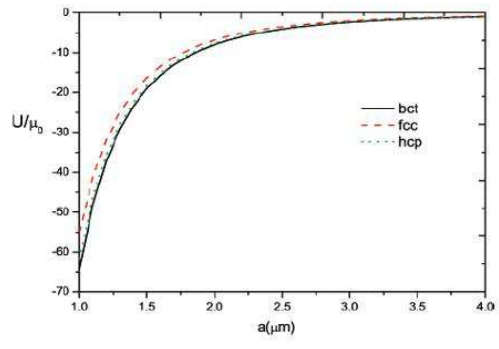


FIG. 5: Jian, Gao, Huang, and Tao

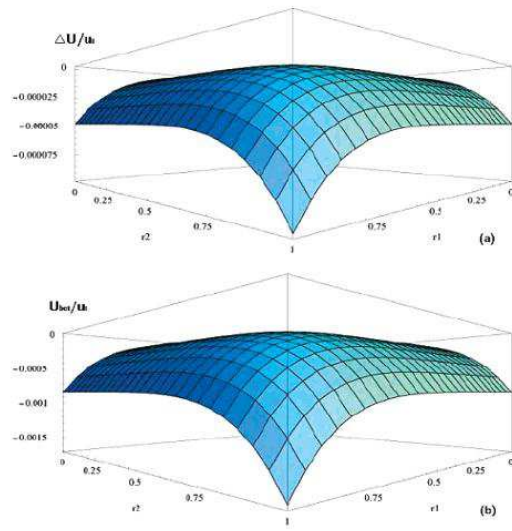


FIG. 6: Jian, Gao, Huang, and Tao

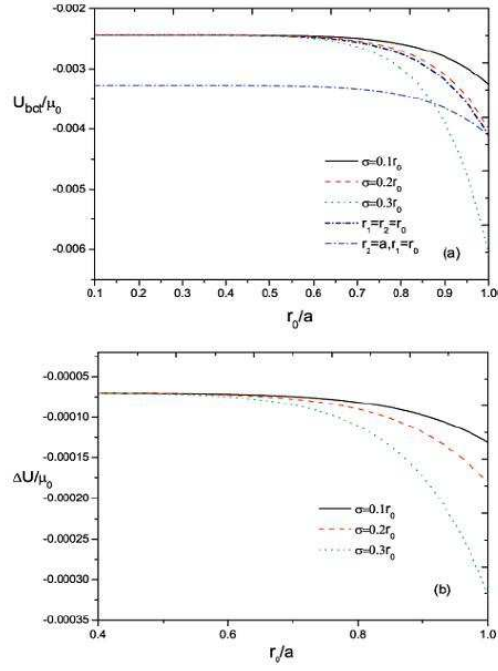


FIG. 7: Jian, Gao, Huang, and Tao

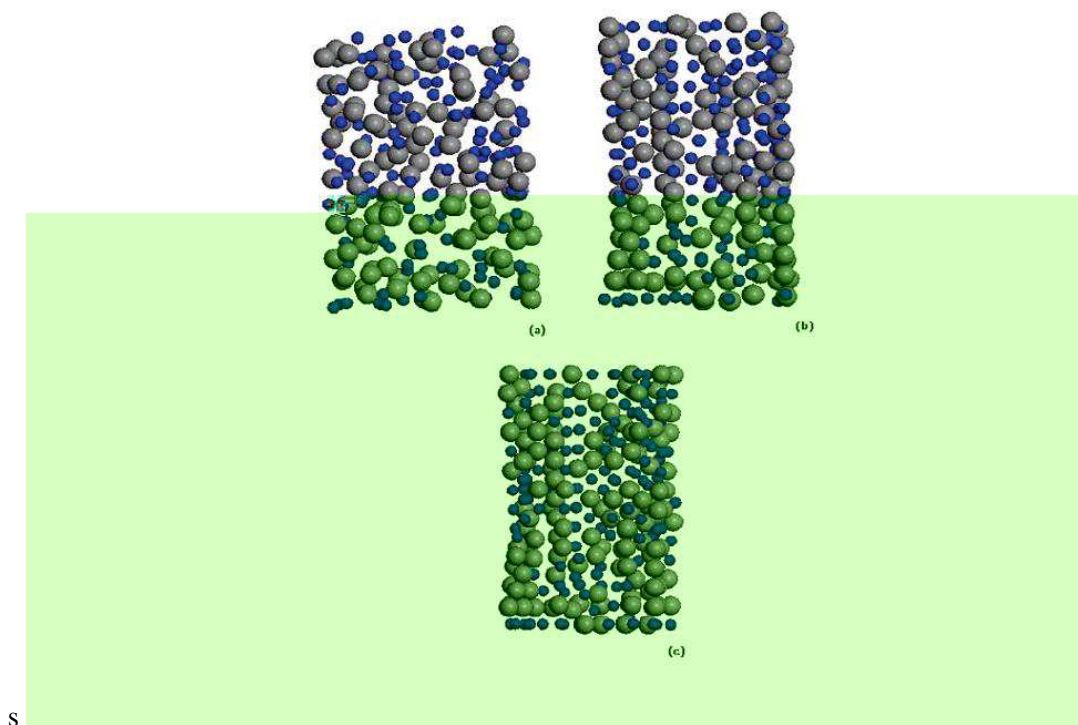


FIG. 8: Jian, Gao, Huang, and Tao